A Journal of the Gesellschaft Deutscher Chemiker

Angewandte International Edition Chemie

GDCh

www.angewandte.org

Accepted Article

Title: H2O-Mediated Synthesis of Superionic Halide Solid Electrolyte

Authors: Xueliang Sun, Xiaona Li, Jianwen Liang, Ning Chen, Jing Luo, Keegan Adair, Changhong Wang, Mohammad Norouzi Banis, Tsun-Kong Sham, Li Zhang, Shangqian Zhao, Shigang Lu, Huan Huang, and Ruying Li

To be cited as: *Angew. Chem. Int. Ed.* 10.1002/anie.201909805
Angew. Chem. 10.1002/ange.201909805

Link to VoR: http://dx.doi.org/10.1002/anie.201909805
http://dx.doi.org/10.1002/ange.201909805

WILEY-VCH

10.1002/anie.201909805

WILEY-VCH

COMMUNICATION

H_2O-Mediated Synthesis of Superionic Halide Solid Electrolyte

Xiaona Li,[a]† Jianwen Liang,[a]† Ning Chen,[b] Jing Luo,[a] Keegan R. Adair,[a] Changhong Wang,[a] Mohammad Norouzi Banis,[a, b] Tsun-Kong Sham,[c] Li Zhang,[d] Shangqian Zhao,[d] Shigang Lu,[d] Huan Huang,[e] Ruying Li,[a] and Xueliang Sun[a], *

Abstract: To promote the development of solid-state batteries, polymer, oxide, and sulfide-based solid-state electrolytes (SSEs) have been extensively investigated. However, the disadvantages of these SSEs, such as high-temperature sintering of oxides, air instability of sulfides, and narrow electrochemical windows of polymers electrolytes, significantly hinder their practical application. Therefore, developing SSEs that spontaneously possesses high ionic conductivity (>10^{-3} S cm^{-1}), good-air stability, wide electrochemical window, excellent electrode interface stability, low-cost mass production is highly demanded. Here we report a halide Li^+ superionic conductor, Li_3InCl_6 that can be synthesized in water. Most importantly, the as-synthesized Li_3InCl_6 shows a high ionic conductivity of 2.04×10^{-3} S cm^{-1} at 25 °C. Furthermore, the ionic conductivity can be totally recovered after dissolved in water. Combining with $LiNi_{0.8}Co_{0.1}Mn_{0.1}O_2$ cathode, solid-state lithium batteries shows astonishing cycling stability. The H_2O-mediated synthesis of Li_3InCl_6 can significantly promote the advances of all-solid-state lithium batteries.

All-solid-state lithium batteries (ASSLBs) using solid-state electrolytes (SSEs) are considered as promising next-generation energy storage systems with improved safety due to the elimination of the flammable liquid electrolyte in convention lithium ion batteries.[1] Among the various types of electrolytes, oxide-based and sulfide-based SSEs are considered to be the most promising candidates for use in ASSLBs because of their high ionic conductivity over 10^{-3} S cm^{-1}.[1c, 2] Despite the recent progress made in these SSEs, several serious obstacles are still hindering their practical applications, especially the manufacturing complexity and sensitivity.[3]

For the case of oxide-based SSEs, high sintering temperatures are required both during the synthesis of SSEs and in the subsequent steps to promote intimate contact between electrode materials and SSE, making the manufacturing costly and might cause interfacial reactions.[4] For sulfide-based SSEs, their chemical instability in air and moisture inevitably cause deterioration of structure/composition, leading to a large decrease in ionic conductivity and the release of noxious H_2S gas.[5] Another serious challenge for sulfide SSEs is the unavoidable and detrimental side reactions with high-voltage oxide cathode materials (e.g. $LiCoO_2$ and $LiNi_xMn_yCo_zO_2$).[6] Direct contact between sulfide SSEs and oxide cathode materials results in the formation of a lithium deficient space-charge layer and the diffusion of transition metals from cathode to sulfide SSE which react to the electrolyte and form metal sulfides.[7] In this context, interfacial protection layers between sulfide SSEs and oxide cathodes are necessary but introduce extra complexity and cost for the fabrication process.[6b, 8]

To address these issues, halide SSEs, which were developed in the 1970s, have emerged as attractive alternatives.[9] Unfortunately, the development of halide SSEs has been limited due to their relatively low ionic conductivity and structural instability of some species.[1d, 10] For example, the Li_3YCl_6 synthesized by H. D. Lutz et al. in 1992 only achieved an ionic conductivity of ~10^{-4} S cm^{-1} at 200 °C.[9a] Although high-temperature phase Li_3InBr_6 has a high ionic conductivity of 10^{-3} S cm^{-1} at 25 °C, the as-prepared Li_3InBr_6 shows quite low ionic conductivity of 10^{-7} S cm^{-1} and its structure will be destroyed at -13 °C.[11] In more recent times, the relatively stable Li_3YCl_6 and Li_3YBr_6 SSEs with high ionic conductivities of ~10^{-3} S cm^{-1} were synthesized by Tetsuya Asano et al. using a high-energy ball milling and high-temperature annealing process.[12] Nevertheless, these Li^+-conducting halide SSEs are still sensitive to moisture.[10, 13]

Simultaneously achieving high ionic conductivity, high stability toward oxide cathodes, moisture resistance, and a water-based synthesis method would be an ultimate goal for halide SSEs. In the present study, we report a halide-based SSE, Li_3InCl_6 that can be synthesized via a H_2O-mediated route (eq 1). The reaction between LiCl and $InCl_3$ can be mediated by H_2O at room temperature to form $Li_3InCl_6{\cdot}xH_2O$, and the removal of H_2O affords pure Li_3InCl_6 and recovered conductivity (**Figure 1**). The Li_3InCl_6 SSE possesses a high ionic conductivity of 2.04×10^{-3} S cm^{-1} at 25 °C and good chemical/electrochemical stability toward traditional oxide cathodes. This halide SSE delivered essential advantages over commercial sulfide-SSEs in terms of synthetic simplicity, air/humidity stability, and direct compatibility (both chemically and electrochemically) with oxide cathodes. Excellent electrochemical performance is demonstrated in ASSLBs assembled with $LiNi_{0.8}Mn_{0.1}Co_{0.1}O_2$ cathode.

[a] Dr. X. Li, Dr. J. Liang, J. Luo, K. Adair, C. Wang, Dr. M. Banis, Dr. R. Li, Prof. X. Sun
Department of Mechanical and Materials Engineering, University of Western Ontario, 1151 Richmond St, London, Ontario, N6A 3K7, Canada
E-mail: xsun9@uwo.ca
[b] Dr. N. Chen, Dr. M. Banis,
Canadian Light Source, 44 Innovation Boulevard, Saskatoon, SK S7N 2V3, Canada
[c] Prof. T. Sham
Department of Chemistry, University of Western Ontario, 1151 Richmond St, London, Ontario, N6A 3K7, Canada
[d] Dr. S. Zhao, Dr. L. Zhang, Dr. S. Lu,
China Automotive Battery Research Institute Co. Ltd, 5th Floor, No. 43, Mining Building, North Sanhuan Middle Road, Beijing, China, 100088
[e] Dr. H. Huang,
Glabat Solid-State Battery Inc., 700 Collip Circle, London, ON, N6G 4X8, Canada
† These authors contribute equally to this work.

Supporting information for this article is given via a link at the end of the document.((Please delete this text if not appropriate))

10.1002/anie.201909805

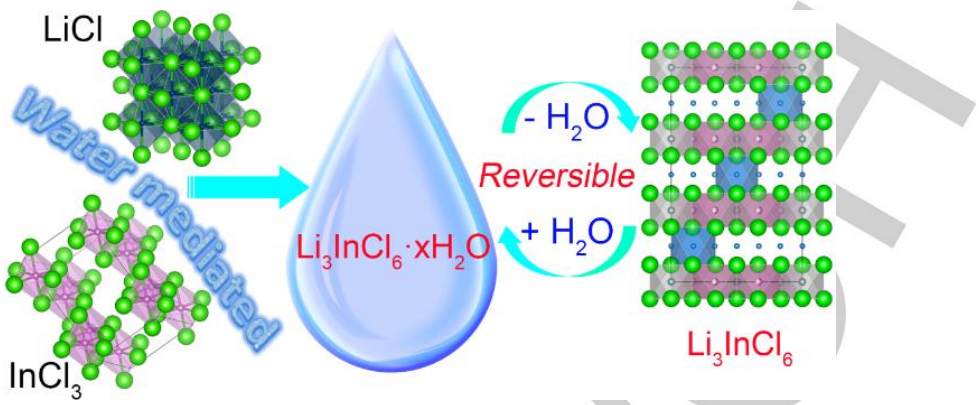

Figure 1. Illustration of water-mediated synthesis route for Li_3InCl_6 SSE and the reversible conversion between the hydrated a $Li_3InCl_6{\cdot}xH_2O$ and dehydrated Li_3InCl_6.

Li_3InCl_6 SSE was synthesized from a H_2O-mediated route from precursors in water (eq 1). Typically, commercial LiCl and $InCl_3$ precursors with a molar ratio of 3:1 were dissolved in water. After evaporation of the water, the product was highly crystalline as shown in Figure S1. The corresponding X-ray diffraction (XRD) patterns were not matched to any particular chemicals including LiCl, $InCl_3$, $InCl_3{\cdot}xH_2O$, and Li_3InCl_6. The obtained product was probably a hydrated form of lithium indium chloride as $Li_3InCl_6{\cdot}xH_2O$ similar to other indium halide hydrates such as $Cs_2InBr_5{\cdot}H_2O$,[14] $(NH_4)_2InCl_5{\cdot}H_2O$[15] and $K_3InCl_6{\cdot}nH_2O$[15]. Coordinating water was confirmed by Fourier transform infrared spectroscopy (Figure S2). The number of coordinated water (x in $Li_3InCl_6{\cdot}xH_2O$) was estimated to be 2 by thermogravimetric analysis (TGA, Figure S3). Different dehydration temperatures from 100 to 200 °C were chosen for post-treatment based on the TGA curves.

$$3LiCl + InCl_3 \xrightarrow{H2O} Li_3InCl_6{\cdot}xH_2O \xrightarrow{\Delta} Li_3InCl_6 \quad (1)$$

After heating the $Li_3InCl_6{\cdot}2H_2O$ under vacuum at 200 °C for 4 h, the dehydrated sample was obtained. The corresponding XRD pattern shown in Figure S4 can be indexed to Li_3InCl_6. The XRD patterns of other samples obtained from dehydration attempts at lower vacuum temperatures of 100 and 130 °C are shown in Figure S5. The dehydrated form of Li_3InCl_6 can also be obtained through a dehydration process in air or Ar, while an impurity phase of InOCl appeared (Figure S6, S7). Thus, the dehydration process was conducted under vacuum to ensure high purity. From an energy sustainable and ease of handling point of view, the facile aqueous synthetic route for Li_3InCl_6 is extremely attractive compared to the conventional high-energy and expensive ball-milling and high temperature annealing process required for other SSEs.[12]

The ionic conductivity of the Li_3InCl_6 SSE obtained at 200 °C was studied by electrochemical impedance spectroscopy (**Figure 2**a). The plotted ionic conductivities were calculated from the sum of the grain boundary and bulk resistance featured with a semicircle in the high frequency region as presented in the inset of Figure 2a. The ionic conductivity of Li_3InCl_6 is 2.04×10^{-3} S cm^{-1} at 25 °C, which is among the best reported halide SSEs.[9a, 10, 12, 16] The corresponding activation energy (E_a) calculated based on the Arrhenius equation[1d] is 0.347 eV. The electronic conductivity ($\sigma_{dc\text{-}electron}$) of Li_3InCl_6 was determined to be 1.86×10^{-9} S cm^{-1} by a direct current (DC) polarization measurement[17] (Figure S8). The low value of electronic conductivity compared to the ionic contribution makes it good SSE candidate for practical application.[18] The electrochemical stability of the Li_3InCl_6 SSE was evaluated by cyclic voltammetry (CV) with a Li/Li_3InCl_6/Au cell at 25 °C (Figure 2b). The cell displayed reversible cathodic and anodic current response around 0 V, which is similar to other SSEs reported previously, [19] and further displays that Li_3InCl_6 is not stable towards Li metal. Favorably, the absence of oxidation currents at high voltages indicated a practical electrochemical stability.[20] The ionic conductivities and activation energies of Li_3InCl_6 SSEs obtained at 100 and 130 °C under vacuum are also compared in Figure S9 and Table S1. Clearly, the ionic conductivity of the Li_3InCl_6 obtained at 200 °C is at its highest. Moreover, the synthesis of Li_3InCl_6 SSEs can be easily scale-up to 110 g through the H_2O-mediated synthesis route with high purity and ionic conductivity (1.54×10^{-3} S cm^{-1} at 25 °C) as shown in Figure S10.

10.1002/anie.201909805

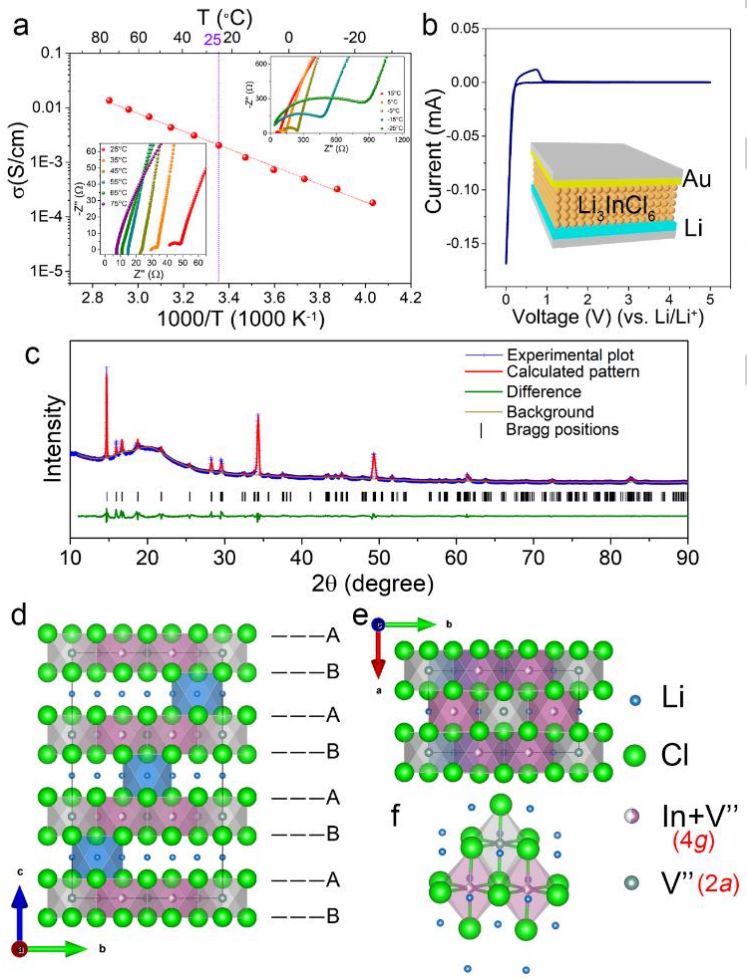

Figure 2. (a) Impedance plots of the conductivity data from low to high temperatures and Arrhenius conductivity plots of Li_3InCl_6 SSEs. (b) Cyclic voltammogram of Li/Li_3InCl_6/Au cell vs. Li/Li^+ from 0 to 5.0 V at a scan rate of 0.1 mV s^{-1}. (c) Representative X-ray diffraction pattern of Li_3InCl_6 and the corresponding Rietveld refinements. Structure of Li_3InCl_6. (d,e) Layered structure observed from the view of perpendicular to a-axis, Li^+ (blue), In^{3+} (purple) and vacancy (V'', grey); green balls are Cl^-. (f) Typical Li^+ location around $InCl_6^{3-}$ octahedron.

Figure 2c presents a low scan powder XRD and crystal structure with Rietveld refinement of the Li_3InCl_6 sample that belongs to monoclinic symmetry (space group C2/m). The structure was refined using the Rietveld method combined with the DFT Geometry Optimization calculation.[21] Table S2,3 shows the detailed structural information of the Rietveld refinement results, which reveal a different structure to that of Li_3InCl_6 in the database (ICSD No. 04-009-9027, Table S4). The distorted rock-salt structure of Li_3InCl_6 (Figure 2d-f) exhibits an AB AB Cl^- packing with both Li^+ and In^{3+} ions in the octahedral sites ($LiCl_6$ and $InCl_6$ octahedra) and vacancies in two independents octahedral sites (V"Cl_6 octahedron, V" is vacancy). The vacancy in the 4*g* site (V"$_{4g}$) is shared with In^{3+} and the vacancy occupation is around 47%. In contrast, the vacancy of the 2*a* site (V"$_{2a}$) shows 100% occupation. From the symmetry and electrostatic point of view, the V"$_{2a}$ site is expected to be more stable than the site of V"$_{4g}$. Meanwhile, DFT calculation further confirms the lower energy in the vacancy formation of V"$_{2a}$ than V"$_{4g}$. Thus, the vacancy distribution within the synthesized Li_3InCl_6 is quite different from that of the database, indicating that different Li^+ conduction and migration properties may be present since those vacancies are highly related to the ionic conductivity.[22]

10.1002/anie.201909805

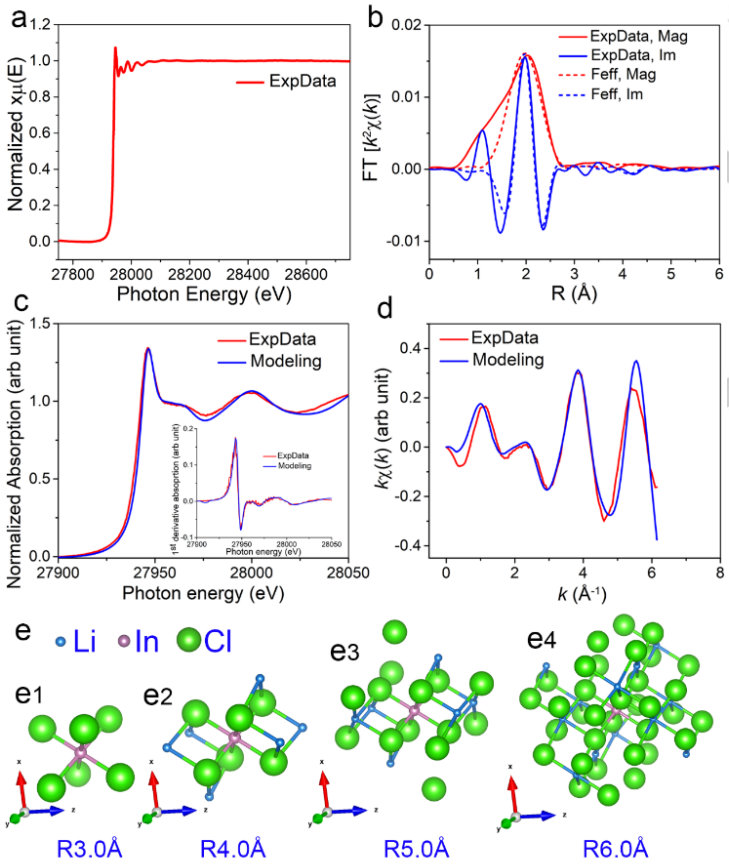

Figure 3. (a) XAS spectra of Li_3InCl_6. (b) R space curve fitting result, comparison is made between experimental data and Feff modeling in terms of magnitude of FT (red solid and red dash traces for the experimental data and the Feff modeling, respectively) and the imaginary part of FT (blue solid and blue dash traces for the experimental data and the Feff modeling, respectively). The comparison between XANES modeling and experimental data in (c) XANES spectra (corresponding first derivative spectra presented in insert), and (d) for $k\chi(k)$. (e1-e4) The XAFS model M-2 structural system based on the crystallography of Li_3InCl_6 after DFT calculation and X-ray refinement. The system is composed by In centered spherical clusters with the radius progressively increasing from 3.0 Å to 6.0 Å.

Furthermore, indium K-*edge* X-ray absorption fine structure (XAFS) was employed to further reveal the detailed structure of the Li_3InCl_6. The XAFS model M-1 (the first model) was developed based on the crystallographic structure of Li_3InCl_6 in the database, theoretical modeling and further verified by the Rietveld refinement upon XRD of the synthesized Li_3InCl_6 (**Figure 3** a-d). The shell by shell local structural around the indium center of the original structural model was divided into a three shells model, incorporating backscattering from neighbouring atoms with an interatomic distance up to ~5.0 Å, which is roughly equivalent to the typical EXAFS detection limit (Table S5). A Gaussian window function was used for Fourier transform (FT) during fitting (detailed information shown in supporting information).[23] The Feff R space fitting result is compared to the experimental data, revealing an overall matching in both magnitude and imaginary part of the FT with certain fitting for the R region shorter than ~1.4 Å (Figure 3b), which is also proved by the comparison of k space for $k^2\chi(k)$ results (Figure S11). Moreover, the fitted structural parameters (Table S5) are consistent well with the indium local structural environment predicted by crystallography.

The M-2 (the second model) structural system was developed based on the same crystallography data of Li_3InCl_6 used for developing M-1. The radius of the indium centered clusters is progressively increased from the first shell $InCl_6$ octahedron (i.e., R3.0Å, Figure 3e1) to R6.0Å cluster (Figure 3e4), matching the usual XAFS detection capability. The M-2 based theoretical X-ray absorption near edge structure (XANES) spectrum and corresponding first derivative spectrum system are shown in Figure S12. Based on features “A” and “B”, the XANES modeling best-fit was obtained based on the cluster R5.0Å (Figure 3e3). The comparison is made correspondingly among the best-fit versus the experimental data in XANES (Figure 3c), first derivative spectrum (Figure 3c insert), and $k\chi(k)$ (Figure 3d), revealing close agreement between them. This result clearly indicates that the indium local structure environment of the synthesized Li_3InCl_6 SSE is consistent with the result from the DFT theoretical modeling and the XRD Rietveld refinement. The observed particle size of synthesized Li_3InCl_6 SSE (Figure S13) is around several hundreds of nanometers, which consists of aggregates of small Li_3InCl_6 particles.

10.1002/anie.201909805

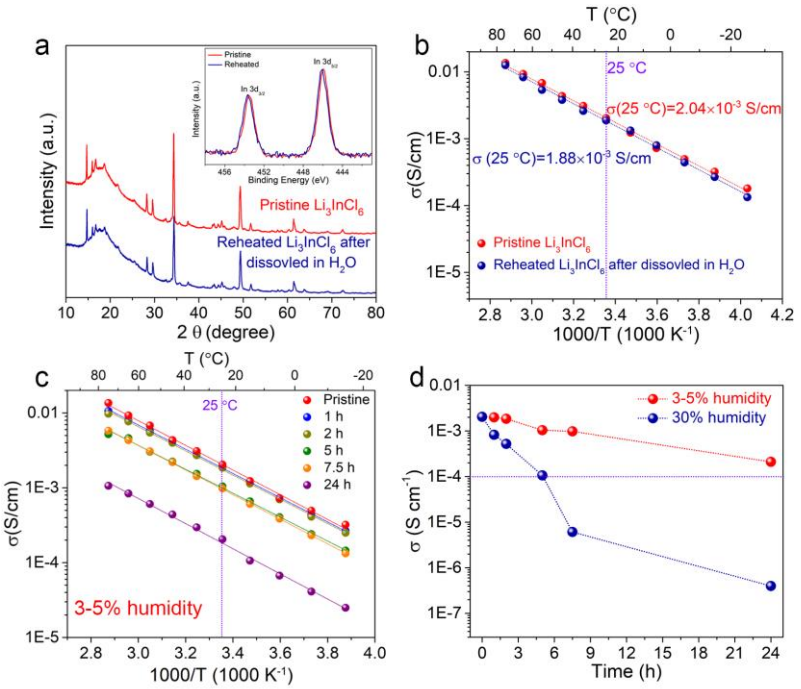

Figure 4. Evaluation of Li_3InCl_6 stability in a humid environment. (a) XRD patterns (In 3d XPS spectra shown in insert) and (b) comparison on the ionic conductivities of the pristine Li_3InCl_6 SSE (red) and a sample completely dissolved in water followed by drying at 200 °C for 1 h under vacuum (blue). (c) Arrhenius plots of Li_3InCl_6 SSE exposed in 3-5% humidity environment at different times. (d) Ionic conductivity evolution of Li_3InCl_6 SSE exposed in 3-5% and 30% humidity environments at different times.

Given that the Li_3InCl_6 SSE can be synthesized through an H_2O-mediated synthesis route directly, we intentionally expose the Li_3InCl_6 SSE to humidity to investigate its stability and recoverability. The influence of humidity was studied by completely dissolving Li_3InCl_6 in deionized water. The pH value of Li_3InCl_6 solution (10 wt%) is about 5, which is similar to the solution of the precursors ($LiCl+InCl_3$, 10 wt%) as shown in Figure S14, 15. The retrieved sample after dissolution in water and drying exhibited a similar XRD pattern to the hydrated form of $Li_3InCl_6{\cdot}2H_2O$ (Figure S16). After heating/dehydration at 200 °C for 1 h under vacuum, the "spoiled" sample was able to fully recover the pristine Li_3InCl_6 structure according to XRD and X-ray photoelectron spectroscopy (XPS) results (**Figure 4**a, S17). The corresponding ionic conductivity and activation energy of the "spoiled" sample were observed to be 1.88×10^{-3} S cm^{-1} (25 °C) and 0.351 eV (Figure 4b), respectively. It can be concluded that, no significant changes in ionic conductivity or activation energy were observed, demonstrating that Li_3InCl_6 SSE possesses good humidity stability with resumable superionic conductivity. The ionic conductivity and structure evolution of Li_3InCl_6 SSE exposed to different humidity of 3-5% and 30% without reheating process were further measured. The ionic conductivity of Li_3InCl_6 SSEs can still achieve over 10^{-3} S cm^{-1} and 10^{-4} S cm^{-1} for 7.5 h and 24 h exposure time in 3-5% humidity, respectively (Figure 4c,d). Even after 24 h exposure, the main XRD patterns can be indexed to pristine Li_3InCl_6 as shown in Figure S18. When increase the humidity to 30%, the conductivity of exposed Li_3InCl_6 reduced a lot along exposure time, with 3.98×10^{-7} S cm^{-1} achieved after 24 h (Figure 4d, S19), which is caused by the easier formation of $Li_3InCl_6{\cdot}2H_2O$ (Figure S20). No other oxidized or hydrolyzed species were observed as supported by XPS results (Figure S21, 22). Both the samples reheated again still recover back to Li_3InCl_6 (Figure S18, 20). The results proved that the dehydration/hydration process between $Li_3InCl_6{\cdot}2H_2O$ and Li_3InCl_6 is reversible under certain conditions.

10.1002/anie.201909805

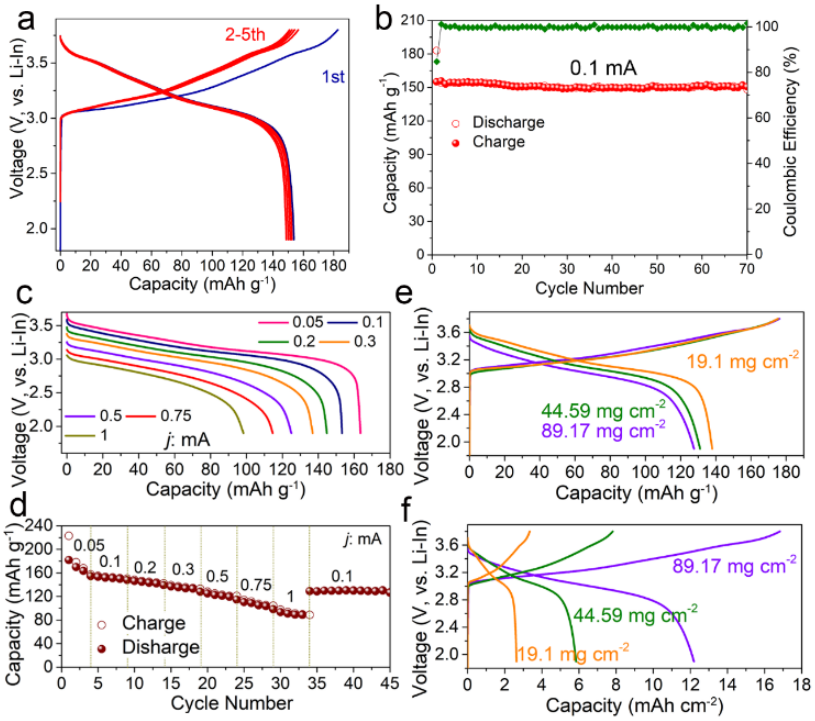

Figure 5. Electrochemical performance of NMC811/Li_3InCl_6/$Li_{10}GeP_2S_{12}$/In all-solid-state cells at 25 °C. (a) Charge-discharge curves and (b) cycling performance of NMC811/Li_3InCl_6/$Li_{10}GeP_2S_{12}$/In cell at 0.1 mA. (c,d) Rate capability of NMC811/Li_3InCl_6/$Li_{10}GeP_2S_{12}$/In cells at 0.05, 0.1, 0.2, 0.3, 0.5, 0.75, and 1 mA. (e,f) Charge-discharge curve of high loading cells. Diameter of the electrode is 10 mm.

The Li_3InCl_6 electrolyte was evaluated as a solid electrolyte for practical ASSLBs. **Figure 5**a shows the charge-discharge curves of the assembled ASSLBs using $LiNi_{0.8}Mn_{0.1}Co_{0.1}O_2$ (NMC811)/Li_3InCl_6 as the cathode (SEM and energy dispersive X-ray mapping images shown in Figure S23), Li_3InCl_6 as the electrolyte, and In as the anode between of 1.9-3.8 V vs. LiIn/Li^+ at 0.13 mA cm^{-2} (25 °C, with active NMC811 loading of 8.92 mg cm^{-2}). A thin $Li_{10}GeP_2S_{12}$ layer was set between Li_3InCl_6 and In anode. The ASSLB exhibited a reversible capacity over 154 mAh g^{-1}. A high initial Coulombic Efficiecy of 84.2% was achieved, which is among the best reported for NMC811 cathodes in ASSLBs. [1c, 7a, 8, 24] Stable cycling performance was achieved for 70 cycles, with a reversible capacity of 150 mAh g^{-1} maintained. Good rate capability was also demonstrated as shown in Figure 5c,d. Comparatively, the capacity of ASSLBs with $Li_{10}GeP_2S_{12}$ as electrolyte at ~1.27 mA cm^{-2} is near 0 presented in reference.[7a] Furthermore, ASSLBs with thick electrode configurations were also evaluated (Figure 5e,f). Three ASSLBs with NMC811 loadings of 19.1, 44.59, and 95.54 mg cm^{-2} were assembled, with reversible areal capacity of 2.64, 5.85, and 12.16 mAh cm^{-2}. The corresponding initial Coulombic Efficiency is 78.86, 74.9% and 72.2%, which is comparable to reported NMC811 with much lower areal capacity ASSLBs. The well overlapped In L_3-edge and Cl K-edge XANES spectra of Li_3InCl_6 SSE at different charge/discharge status presented in Figure S24 proves the stability of Li_3InCl_6 SSE with NMC811 during cycling. The high interfacial stability of Li_3InCl_6/NMC811 was further reflected from the impedance evolution of the cell during charge/discharge process (Figure S25). Moreover, even the ASSLB with reheated Li_3InCl_6 as the electrolyte or Li metal as the anode can exhibit stable cycling (Figure S26, 27). The results demonstrate that Li_3InCl_6 is applicable as a practical electrolyte for ASSLBs. Most importantly, the H_2O-mediated synthesis route can be also extended to prepare other ionic conductors such as Na_3InCl_6 (Figure S28).

In summary, halide-based Li^+ superionic conductor, Li_3InCl_6, is successfully prepared by a facile and scalable H_2O-mediated synthesis route, which can be highly favorable for practical manufacturing. A high Li^+ conductivity of 2.04×10^{-3} S cm^{-1} is achieved at 25°C. The reversible conversion between Li_3InCl_6 and $Li_3InCl_6{\cdot}2H_2O$ enables its intrinsic stability with air and humidity, thus ensuring resumable high ionic conductivity. Meanwhile, Li_3InCl_6 is chemically and electrochemically stable in direct contact with high voltage oxide cathode materials (e.g. NMC811). Good performance is demonstrated for ASSLBs using Li_3InCl_6 SSE with NMC811 cathode. Our results suggest that Li_3InCl_6 is a highly promising SSE candidate for practical ASSLBs and sustainable energy storage.

Acknowledgements

This research was supported by Natural Sciences and Engineering Research Council of Canada (NSERC), GLABAT Solid-State Battery Inc., Chian Automotive Battery Research Institute Co. Ltd, Canada Research Chair Program (CRC), Canada Foundation for Innovation (CFI), Ontario Research Fund, the Canada Light Source at University of Saskatchewan (CLS), Canada MITACS fellow, and University of Western Ontario.

Keywords: halide solid electrolyte • air stable • aqueous synthesis • all-solid-state battery • ionic conductivity

[1] aY. Kato, S. Hori, T. Saito, K. Suzuki, M. Hirayama, A. Mitsui, M. Yonemura, H. Iba, R. Kanno, *Nat. Energy* **2016**, *1*, 16030; bY. Ding, Z. P. Cano, A. Yu, J. Lu, Z. Chen, *Electrochem.Energy Rev.* **2019**, *2*, 1-28; cM. A. Kraft, S. Ohno, T. Zinkevich, R. Koerver, S. P. Culver, T. Fuchs, A. Senyshyn, S. Indris, B. J. Morgan, W. G. Zeier, *J. Am. Chem. Soc.* **2018**, *140*, 16330-16339; dJ. C. Bachman, S. Muy, A. Grimaud, H.-H. Chang, N. Pour, S. F. Lux, O. Paschos, F. Maglia, S. Lupart, P. Lamp, *Chem. Rev.* **2015**, *116*, 140-162.

[2] aN. Kamaya, K. Homma, Y. Yamakawa, M. Hirayama, R. Kanno, M. Yonemura, T. Kamiyama, Y. Kato, S. Hama, K. Kawamoto, A. Mitsui, *Nat. Mater.* **2011**, *10*, 682; bL. Nazar, P. Adeli, J. D. Bazak, K.-H. Park, I. Kochetkov, A. Huq, G. Goward, *Angew. Chem. Int. Ed.* **2019**, 58, 8681-8686; cY. Sun, K. Suzuki, S. Hori, M. Hirayama, R. Kanno, *Chem. Mater.* **2017**, *29*, 5858-5864.

[3] Z. Zhang, Y. Shao, B. Lotsch, Y.-S. Hu, H. Li, J. Janek, L. F. Nazar, C.-W. Nan, J. Maier, M. Armand, *Energy Environ. Sci.* **2018**, *11*, 1945-1976.

[4] aX. Han, Y. Gong, K. K. Fu, X. He, G. T. Hitz, J. Dai, A. Pearse, B. Liu, H. Wang, G. Rubloff, *Nat. Mater.* **2017**, *16*, 572; bM. Kotobuki, H. Munakata, K. Kanamura, Y. Sato, T. Yoshida, *J. Electrochem. Soc.* **2010**, *157*, A1076-A1079.

[5] aH. Muramatsu, A. Hayashi, T. Ohtomo, S. Hama, M. Tatsumisago, *Solid State Ionics* **2011**, *182*, 116-119; bT. Ohtomo, A. Hayashi, M. Tatsumisago, K. Kawamoto, *J. Mater. Sci.* **2013**, *48*, 4137-4142.

[6] aJ. Auvergniot, A. Cassel, J.-B. Ledeuil, V. Viallet, V. Seznec, R. m. Dedryvère, *Chem. Mater.* **2017**, *29*, 3883-3890; bW. Zhang, D. A. Weber, H. Weigand, T. Arlt, I. Manke, D. Schröder, R. Koerver, T. Leichtweiss, P. Hartmann, W. G. Zeier, *ACS Appl. Mater. Interfaces* **2017**, *9*, 17835-17845; cS. P. Culver, R. Koerver, W. G. Zeier, J. Janek, *Adv. Energy Mater.* **2019**, 1900626.

[7] aR. Koerver, I. Aygün, T. Leichtweiß, C. Dietrich, W. Zhang, J. O. Binder, P. Hartmann, W. G. Zeier, J. r. Janek, *Chem. Mater.* **2017**, *29*, 5574-5582; bH. Visbal, Y. Aihara, S. Ito, T. Watanabe, Y. Park, S. Doo, *J. Power Sources* **2016**, *314*, 85-92; cG. Oh, M. Hirayama, O. Kwon, K. Suzuki, R. Kanno, *Chem.Mater.* **2016**, *28*, 2634-2640.

[8] Y. J. Nam, D. Y. Oh, S. H. Jung, Y. S. Jung, *J. Power Sources* **2018**, *375*, 93-101.

[9] aH. J. Steiner, H. Lutz, *Z. Anorg. Allg. Chem.* **1992**, *613*, 26-30; bW. Schmidt, H. Lutz, *Ber. Bunsenges. Phys. Chem.* **1984**, *88*, 720-723; cR. Kanno, Y. Takeda, M. Mori, O. Yamamoto, *Chem. Lett.* **1987**, *16*, 1465-1468; dW. Weppner, R. Huggins, *J. Electrochem.Soc.* **1977**, *124*, 35-38.

[10] A. Manthiram, X. Yu, S. Wang, *Nature Reviews Materials* **2017**, *2*, 16103.

[11] aK. Yamada, K. Iwaki, T. Okuda, Y. Tomita, in *Solid State Ionics: Trends in the New Millennium*, World Scientific, **2002**, pp. 621-628; bY. Tomita, H. Nishiyama, K. Kobayashi, Y. Kohno, Y. Maeda, K. Yamada, *ECS Trans.* **2009**, *16*, 137-141.

[12] T. Asano, A. Sakai, S. Ouchi, M. Sakaida, A. Miyazaki, S. Hasegawa, *Adv. Mater.* **2018**, *30*, 1803075.

[13] R. Nagel, T. W. Groß, H. Günther, H. Lutz, *J. Solid State Chem.* **2002**, *165*, 303-311.

[14] L. Zhou, J.-F. Liao, Z.-G. Huang, J.-H. Wei, X.-D. Wang, W.-G. Li, H.-Y. Chen, D.-B. Kuang, C.-Y. Su, *Angew. Chem. In. Ed.* **2019**, 58, 5277-5281.

[15] O. Knop, T. S. Cameron, D. Adhikesavalu, B. R. Vincent, J. A. Jenkins, *Can. J. Chem* **1987**, *65*, 1527-1556.

[16] Y. Tomita, H. Matsushita, H. Yonekura, Y. Yamauchi, K. Yamada, K. Kobayashi, *Solid state ionics* **2004**, *174*, 35-39.

[17] X. Li, J. Liang, X. Li, C. Wang, J. Luo, R. Li, X. Sun, *Energy Environ. Sci.* **2018**, *11*, 2828-2832.

[18] F. Han, A. S. Westover, J. Yue, X. Fan, F. Wang, M. Chi, D. N. Leonard, N. J. Dudney, H. Wang, C. Wang, *Nat. Energy* **2019**, 1.

[19] N. Kamaya, K. Homma, Y. Yamakawa, M. Hirayama, R. Kanno, M. Yonemura, T. Kamiyama, Y. Kato, S. Hama, K. Kawamoto, *Nat. Mater.* **2011**, *10*, 682.

[20] S. Wang, Q. Bai, A. M. Nolan, Y. Liu, S. Gong, Q. Sun, Y. Mo, *Angew. Chem. In. Ed.* **2019**, 58, 8039-8043.

[21] aJ. Rodríguez-Carvajal, *Phys. B: Condens. Matter* **1993**, *192*, 55-69; bV. Favre-Nicolin, R. Černý, *J. Appl. Crystallogr.* **2002**, *35*, 734-743; cS. J. Clark, M. D. Segall, C. J. Pickard, P. J. Hasnip, M. I. Probert, K. Refson, M. C. Payne, *Z. Krist-Cryst. Mater.* **2005**, *220*, 567-570.

[22] N. Adelstein, B. C. Wood, *Chem. Mater.* **2016**, *28*, 7218-7231.

[23] J. J. Rehr, R. C. Albers, *Rev. Mod. Phys.* **2000**, *72*, 621.

[24] F. Strauss, T. Bartsch, L. de Biasi, A.-Y. Kim, J. r. Janek, P. Hartmann, T. Brezesinski, *ACS Energy Lett.* **2018**, *3*, 992-996.

10.1002/anie.201909805

WILEY-VCH

Entry for the Table of Contents (Please choose one layout)

Layout 1:

COMMUNICATION

A superionic conductor of Li_3InCl_6, with room-temperature Li^+ conductivity of 2.04 × 10^{-3} S cm^{-1}, is successfully prepared by a facile and scalable water-mediated synthesis route (3LiCl + $InCl_3$ $\xrightarrow{H2O}$ $Li_3InCl_6{\cdot}xH_2O$ $\xrightarrow{\Delta}$ Li_3InCl_6). The reversible conversion between Li_3InCl_6 and $Li_3InCl_6{\cdot}2H_2O$ enables its intrinsic stability toward air and humidity, thus ensuring resumable high ionic conductivity.

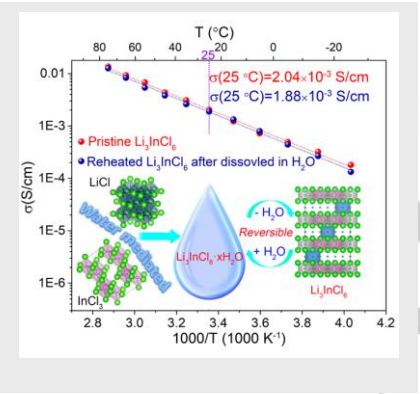

*Xiaona Li, Jianwen Liang, Ning Chen, Jing Luo, Keegan R. Adair, Changhong Wang, Mohammad Norouzi Banis, Tsun-Kong Sham, Li Zhang, Shangqian Zhao, Shigang Lu, Huan Huang, Ruying Li, and Xueliang Sun**

Page No. – Page No.

H_2O-Mediated Synthesis of Superionic Halide Solid Electrolyte